Tailoring Self-Assembled Metallic Photonic Crystals for Modified Thermal Emission

S. E. Han,[1] Andreas Stein,[2] and D. J. Norris[1,*]

[1]*Department of Chemical Engineering and Materials Science, University of Minnesota, Minneapolis, Minnesota 55455, USA*
[2]*Department of Chemistry, University of Minnesota, Minneapolis, Minnesota 55455, USA*

(Received 28 March 2007; revised manuscript received 14 June 2007; published 2 August 2007)

We predict that modified thermal emission can result from three-dimensional, self-assembled photonic crystals. In previous tungsten structures, known as inverse opals, strong absorption prevented any influence of the periodicity. We consider the origin of this effect and show how to tailor both absorption and surface coupling in experimentally realizable metallic inverse opals. Calculations for tungsten, molybdenum, and tantalum crystals show that their optical properties can be similar to or even better than the tungsten woodpile, where modified thermal emission has already been seen.

DOI: 10.1103/PhysRevLett.99.053906 PACS numbers: 42.70.Qs, 44.40.+a

A photonic crystal is a structure that is three-dimensionally periodic on an optical length scale [1]. This periodicity can affect not only the optical transmission and reflection of the material, but also its thermal emission [2]. For example, a specific photonic crystal, the tungsten woodpile structure, has exhibited modified thermal emission when heated [3,4]. This arises because the photonic density of states is altered in the crystal. While the full implications of this effect and its relationship to Planck's blackbody limit are still under discussion [5–9], the potential for these crystals to suppress emission at certain wavelengths (e.g., unwanted heat) is clear. They may allow more efficient emission sources and thermophotovoltaic systems to be obtained.

Unfortunately, the woodpile structure (Fig. 1, inset) requires a complex fabrication process, which has limited its use in the study of thermal emission. A simpler approach would be to use self-assembly. Micrometer-scale colloidal spheres can be organized as a thin face-centered cubic (fcc) crystal on a substrate [10]. The crystal can then be infiltrated and the spheres removed to obtain a structure, known as an inverse opal, in which an fcc array of air spheres is embedded in a film [11–14]. Indeed, tungsten inverse opals have recently been made [15,16], and these could be used to study thermal emission. However, these crystals suffered from extremely strong optical absorption. Essentially, propagating light is absorbed before it senses the periodic structure, eliminating any influence of the photonic crystal. While Kirchhoff's law states that absorption is needed for thermal emission, clearly the absorption should not be severe. If it is, modification of thermal emission by the photonic crystal will not occur. Thus, previous work suggested that inverse opals were ill-suited for studying thermal emission.

Here, we reexamine inverse opals for thermal emission. Namely, we seek to understand the severe absorption in these structures, and to determine if it is intrinsic or can be moderated. For thermal emission modification, the absorption should be significant, but not so strong that the periodicity does not play a role. Previously, thermal emission was treated theoretically for silicon inverse opals [17]. Here, as in the woodpile studies, we begin with tungsten. Because of its extremely high melting temperature (3414°C), tungsten structures allow thermal emission to be studied over a broad temperature range. We then consider other refractory metals such as molybdenum and tantalum. Surprisingly, we find that small, experimentally realizable changes in metallic inverse opals can lead to properties that are very similar to or even better than the tungsten woodpile. Thus, these new structures, which are easily prepared, have great potential for both thermal emission studies and applications.

We begin by calculating the photonic band diagram and optical spectra for the tungsten woodpile using the transfer matrix formalism [18,19]. The results, shown in Fig. 1, were obtained for the structure reported previously [4], except our crystal is 10 layers thick. Unless stated other-

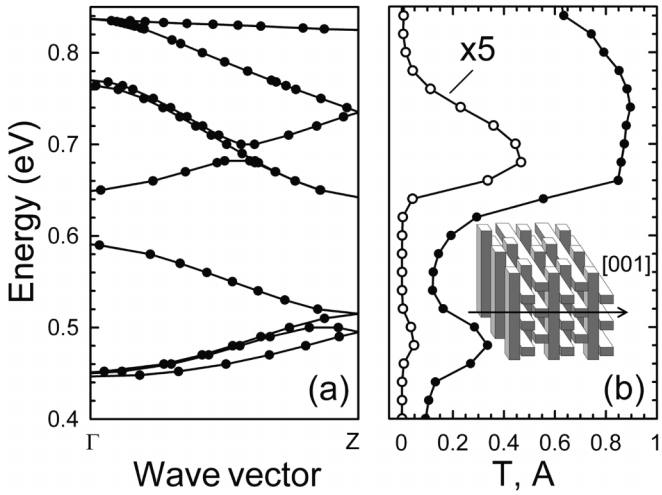

FIG. 1. Calculated (a) photonic band structure and (b) transmittance T (open circles) and absorptance A (solid circles) along [001] for a 10-layer tungsten woodpile (see inset). The rod width, height, and spacing are 0.5, 0.75, and 1.5 μm, respectively, so that the total thickness is 7.5 μm. No bands exist below 0.4 eV. T values are scaled by a factor of 5.

wise, we used the actual complex dielectric function of all metals in this work [20], but the imaginary part was set to zero in all band structure calculations. From the band diagram [Fig. 1(a)] we can identify two groups of bands, one below 0.6 and the other above 0.64 eV. The two peaks in absorption [Fig. 1(b)] correspond to these two groups. Previous thermal emission experiments [4] utilized the upper frequency peak, which is stronger. In this frequency range, transmission is appreciable, suggesting that light is not severely damped but rather interacting with the periodic structure.

To determine whether tungsten inverse opals can exhibit similar optical behavior, we need physical intuition about the origin of the absorption. Then, perhaps we can increase the spatial decay length via small structural changes. Following Krokhin and Halevi [21], we consider an infinite photonic crystal composed of a weakly dissipating material m and air a. The complex magnetic field in the nth photonic band takes the Bloch form

$$\boldsymbol{H}_{\boldsymbol{k}}^{(n)}(\boldsymbol{r}) = \sum_{\boldsymbol{G}} \boldsymbol{h}_{\boldsymbol{k}}^{(n)}(\boldsymbol{G}) e^{i(\boldsymbol{k}+\boldsymbol{G})\cdot\boldsymbol{r}}, \tag{1}$$

where $\boldsymbol{k}$ is the wave vector, $\boldsymbol{G}$ is the reciprocal lattice vector, and $\boldsymbol{h}$ is the complex orthonormal basis vector,

$$\sum_{\boldsymbol{G}} \boldsymbol{h}_{\boldsymbol{k}}^{*(n)}(\boldsymbol{G}) \cdot \boldsymbol{h}_{\boldsymbol{k}}^{(n')}(\boldsymbol{G}) = \delta_{n,n'}. \tag{2}$$

If we express the dielectric function of the material in complex form as $\varepsilon_m' + i\varepsilon_m''$ and the angular frequency as $\omega' + i\omega''$, then the temporal decay rate ω'' is

$$\omega_n''(\boldsymbol{k}) = \frac{\varepsilon_m''}{2\varepsilon_m'(\varepsilon_m' - 1)}\left[1 - \frac{c^2}{\omega_n'^2(\boldsymbol{k})}\sum_{\boldsymbol{G}}|\boldsymbol{k}+\boldsymbol{G}|^2|\boldsymbol{h}_{\boldsymbol{k}}^{(n)}(\boldsymbol{G})|^2\right] \times \omega_n'(\boldsymbol{k}), \tag{3}$$

with c as the velocity of light [21]. It is useful to rewrite Eq. (3) in terms of the field in real space by using Parseval's theorem and Maxwell's equations such that

$$\frac{\omega_n''(\boldsymbol{k})}{\omega_n'(\boldsymbol{k})} = \frac{\varepsilon_m''}{2\varepsilon_m'(\varepsilon_m' - 1)}\left[1 - \frac{\int_{V_c}|\boldsymbol{D}_{\boldsymbol{k}}^{(n)}(\boldsymbol{r})|^2 d\boldsymbol{r}}{\int_{V_c}|\boldsymbol{H}_{\boldsymbol{k}}^{(n)}(\boldsymbol{r})|^2 d\boldsymbol{r}}\right], \tag{4}$$

where V_c is the volume of the unit cell and $\boldsymbol{D}$ is the complex displacement field, defined as in Eq. (1). Now, we assume that material m is a metal with a magnetic permeability of 1 and $\varepsilon_m' \ll 0$. Moreover, the thickness and radius of curvature of the structured metal are always much greater than the skin depth δ. Then, on separating the unit cell into metal and air parts with volumes V_m and V_a, Eq. (4) becomes approximately

$$\omega_n''(\boldsymbol{k}) \approx -\frac{\varepsilon_m''}{2}\left[\frac{\int_{V_m}|\boldsymbol{E}_{\boldsymbol{k}}^{(n)}(\boldsymbol{r})|^2 d\boldsymbol{r}}{\int_{V_a}|\boldsymbol{E}_{\boldsymbol{k}}^{(n)}(\boldsymbol{r})|^2 d\boldsymbol{r}}\right]\omega_n'(\boldsymbol{k}), \tag{5}$$

where $\boldsymbol{E}$ is the complex electric field, as in Eq. (1). So far, $\boldsymbol{k}$ has been treated as a real quantity. If we now regard $\boldsymbol{k}$ as complex, $\boldsymbol{k}' + i\boldsymbol{k}''$, the spatial decay length is inversely proportional to $\boldsymbol{k}''$ and, in the limit of weak dissipation, $\boldsymbol{k}'' = -\omega''/\boldsymbol{v}_g$, where $\boldsymbol{v}_g$ is the group velocity [21]. Thus, to increase the spatial decay length, we need to increase the group velocity and/or decrease ω''. Equation (5) allows ω'' to be quantified from the distribution of the field. Physically, it states that ω'' is related to the ratio of the field intensity in the metal to that in the air, which, in turn, is roughly proportional to $S_m\delta/V_a$, where S_m is the surface area of the metal in the unit cell. Thus, we need to decrease S_m/V_a by altering the inverse opal structure.

Based on this analysis, we considered several simple alterations to the inverse opal. The most promising involves the insertion of air cylinders into the structure at the contact points between the air spheres. The cylinders are oriented along the lines connecting the centers of the spheres. Outside of these spheres and cylinders, the structure is filled with metal. This alteration is advantageous for three reasons. First, the cylinders decrease S_m/V_a. For example, when the cylinder diameter d is half of the sphere diameter D, S_m/V_a is 52% of its value without the cylinders. Second, the cylinders allow the air spheres to interact, resulting in band broadening and an increase in the group velocity [22]. Finally, and perhaps most importantly, experimental techniques already exist to add such cylinders to inverse opals [16,23].

Figure 2 describes how the optical properties of the metallic inverse opals vary with air cylinder diameter. To obtain these plots we assumed a constant dielectric function with weak absorption and determined the band diagram for the ΓL direction for a range of cylinder diameters [19]. From each such diagram, a lower and upper group of bands could be identified, as in Fig. 1(a). For each group, we then extracted the minimum value of k''/ε_m'' and v_g/c at the same frequency. The resulting plots are useful for two reasons. First, recalling that the spatial decay length is inversely proportional to k'', Fig. 2(b) shows that the spatial decay length increases with cylinder diameter. As k'' is, in turn, inversely proportional to v_g, Fig. 2(a) indicates that this increase is due in part to an increase in the group velocity. Because our goal is to lengthen the spatial decay, these plots suggest that we should use a cylinder with the largest possible diameter. However, the inverse opal becomes disconnected when $d/D > 0.577$. Thus, to ensure mechanical stability we use $d/D = 0.5$ below, corresponding to a reasonable metal filling fraction of 15%. Such a structure is depicted in Fig. S1 in Ref. [19]. Second, the plots in Fig. 2 were constructed to allow comparison with values for the woodpile, shown as horizontal lines. For $d/D = 0.5$, Fig. 2(b) shows that the spatial decay length in the inverse opal should be only slightly shorter than in the woodpile for the upper group of bands. Moreover, it should actually be longer for the lower group of bands. Thus, this plot indicates that absorption in inverse opals can be moderated by inserting air cylinders [24]. Further, the tailored structure may exhibit optical behavior comparable to the woodpile, at least at certain frequencies.

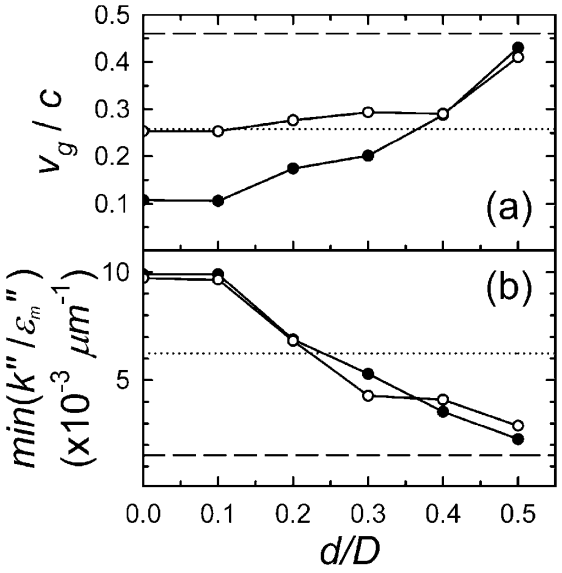

FIG. 2. (a) Normalized group velocity and (b) the minimum of k''/ε_m'' vs d/D along [111] for the inverse opal. These values are extracted from the frequency dependence of k' and k'' in the limit of vanishing ε_m'', as described in Ref. [19]. Results are plotted for the lowest frequency group of bands (solid circles) and the next group of bands (open circles). For comparison, values for the lowest group of bands (dotted line) and the second group of bands (dashed line) for the woodpile are also shown. A constant $\varepsilon_m = -100 + 0.01i$ was used.

Before testing this, we must first consider how light in the structure couples to the external field. This coupling, which also affects the optical properties of the crystal, is determined by both the symmetry of the eigenmodes and the surface geometry. For thin self-assembled colloidal crystals, the external surfaces are typically hexagonally close-packed sheets of spheres that are perpendicular to the ΓL direction. If such a crystal is grown between two substrates and then processed to obtain a freestanding inverse opal, the air cylinders discussed above will also arise at the contact points between the substrates and the outer spheres. Thus, the two external surfaces will be flat metal interfaces perforated by a hexagonal array of cylindrical holes with diameter d. This surface geometry is similar to the metal hole arrays that have been investigated for extraordinary optical transmission [25]. In that case, enhanced transmission occurs near the frequencies of surface plasmons. For normal incidence, the plasmon frequency of a hexagonal hole array is given by

$$\frac{\omega D}{2\pi c} = 2\sqrt{\frac{(i^2 + ij + j^2)(\varepsilon_m' + 1)}{3\varepsilon_m'}}, \qquad (6)$$

where i and j are integers. A transmission peak will be located where $\omega D/2\pi c$ is near 1, corresponding to the lowest surface plasmon frequency modes given by $(i, j) = (\pm 1, 0)$, $(0, \pm 1)$, $(1, -1)$, and $(-1, 1)$.

As in previous studies on two-dimensional photonic crystals [26], we examined how this surface influences the optical properties. The calculated reflectance for the outermost half-layer of the structure, including the air cylinders, is shown in Fig. 3(a) for $\varepsilon_m = -100 + 27i$. A reflectance dip (or transmission peak) occurs near the frequency predicted by Eq. (6). For comparison, Fig. 3(b) shows the calculated band diagram for a tailored inverse opal assuming $\varepsilon_m = -100$. Because the reflection dip of the surface [Fig. 3(a)] overlaps with the upper group of bands, i.e., above $\omega D/2\pi c = 0.8$, one might expect to see the best coupling to the external field in this region for a tailored 5-layer inverse opal. Figure 3(c) shows the calculated reflectance for such a structure with $\varepsilon_m = -100 + 27i$. Indeed, the reflectance dip for the lower group of bands (i.e., at $\omega D/2\pi c = 0.66$) is weaker than one would expect based solely on the spatial decay length discussed above. The surface is effectively blocking the incident light at these frequencies. Thus, below we utilize the upper group of bands, which couple to the external field strongly, even though the spatial decay here is slightly shorter than in the woodpile.

We can then adjust the lattice constant of the crystal to locate the absorption peak in the near-infrared region to compare with the woodpile results. As Fig. 3(c) suggests that the absorption peak in the inverse opal should occur around $\omega D/2\pi c = D/\lambda = 1$, we chose $D = 1.7\ \mu$m to place the peak near this wavelength. Figures 4(a) and 4(b) show results for a tailored 5-layer tungsten inverse opal along the ΓL direction. The absorption peak [Fig. 4(b)] occurs at 0.68 eV or $\lambda = 1.82\ \mu$m. Comparison with Fig. 1(b) reveals that the optical spectra of the tailored tungsten inverse opal are quite similar to those of the tungsten woodpile. The absorption peak of the inverse opal is even narrower, which may be advantageous for

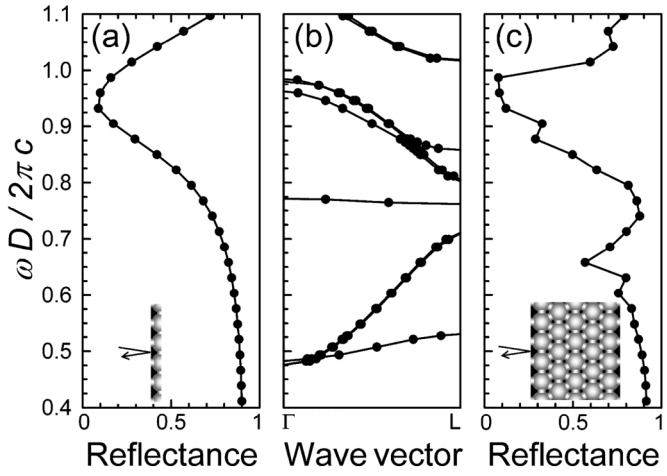

FIG. 3. (a) Calculated reflectance for normal incidence on the top half-layer of the inverse opal with air cylinders, using $\varepsilon_m = -100 + 27i$ and $d/D = 0.5$. (b) Photonic band structure along [111] for an inverse opal with air cylinders, using $\varepsilon_m = -100$ and $d/D = 0.5$. No bands exist below 0.4 eV. (c) Calculated reflectance for normal incidence along [111] for a 5-layer inverse opal as in (b) except $\varepsilon_m = -100 + 27i$. The insets show schematic side views of the structures.

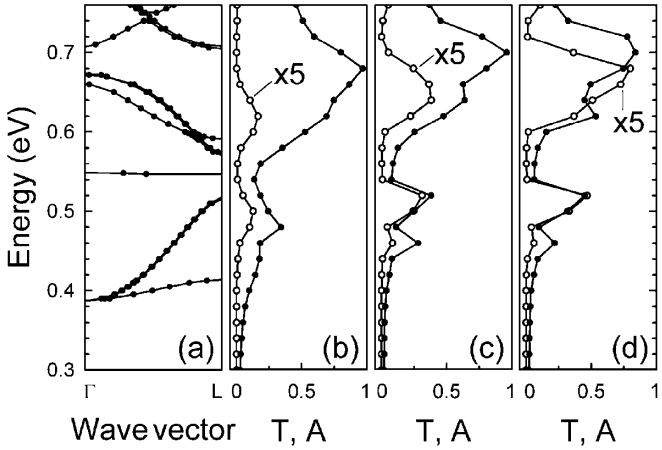

FIG. 4. (a) Calculated photonic band structure and (b) optical transmittance T (open circles) and absorptance A (solid circles) along [111] for a 5-layer tungsten inverse opal with air cylinders. (c),(d) Calculations for analogous structures from molybdenum and tantalum, respectively. For all, we used $D = 1.7$ μm, $d/D = 0.5$. T values are scaled by a factor of 5. In (a) no bands exist below 0.3 eV.

some applications. The maximum transmittance is 0.03 for the tungsten inverse opal, which has a thickness of 7.25 μm, compared to 0.09 for the tungsten woodpile in Fig. 1, which is 7.5 μm thick. The difference in transmittance can be explained by Fig. 2(b), which indicates that the spatial decay length is longer in the woodpile than the tailored inverse opal for the upper group of bands.

To test further our tailored structure, we performed several additional calculations. First, Fig. S2 in Ref. [19] shows the band structure and optical spectra for our tungsten inverse opal along the ΓX direction. These results are quite similar to those for the ΓL direction [Fig. 4(b)], indicating that thermal emission from several external facets of the crystal should act similarly. Second, Figs. 4(c) and 4(d) present optical spectra along the ΓL direction for our tailored inverse opal made from Mo and Ta, respectively. These spectra show that the transmission can be even higher than the tungsten woodpile. Thus, by compromising slightly on the melting temperature of the metal (2622 °C and 3007 °C for Mo and Ta, respectively), even better properties may be possible.

In conclusion, we predict that metallic inverse opals can be tailored to have optical properties similar to or even better than the tungsten woodpile. By inserting air cylinders and considering the coupling to the external field, these inverse opals should exhibit optical absorption that, while still significant, is sufficiently moderated that the periodicity of the photonic crystal will have an effect. Because Kirchhoff's law relates thermal emission directly to absorption, such structures should exhibit modified thermal emission. Moreover, these inverse opals are experimentally realizable and have external surfaces that are convenient for predicting coupling to the external field. Thus, these self-assembled photonic crystals have great potential for experimental studies and applications of modified thermal emission.

This work was supported by the U.S. Department of Energy (No. DE-FG02-06ER46348) using resources at the University of Minnesota Supercomputing Institute. S. E. H. and D. J. N. benefitted from financial support from the Samsung and Humboldt Foundations, respectively.

*dnorris@umn.edu.

[1] J. D. Joannopoulos, P. R. Villeneuve, and S. Fan, Nature (London) **386**, 143 (1997).
[2] C. M. Cornelius and J. P. Dowling, Phys. Rev. A **59**, 4736 (1999).
[3] J. G. Fleming *et al.*, Nature (London) **417**, 52 (2002).
[4] S.-Y. Lin, J. Moreno, and J. G. Fleming, Appl. Phys. Lett. **83**, 380 (2003).
[5] T. Trupke, P. Wurfel, and M. A. Green, Appl. Phys. Lett. **84**, 1997 (2004).
[6] C. Luo *et al.*, Phys. Rev. Lett. **93**, 213905 (2004).
[7] C. H. Seager, M. B. Sinclair, and J. G. Fleming, Appl. Phys. Lett. **86**, 244105 (2005).
[8] I. El-Kady, W. W. Chow, and J. G. Fleming, Phys. Rev. B **72**, 195110 (2005).
[9] W. W. Chow, Phys. Rev. A **73**, 013821 (2006).
[10] P. Jiang *et al.*, Chem. Mater. **11**, 2132 (1999).
[11] B. T. Holland, C. F. Blanford, and A. Stein, Science **281**, 538 (1998).
[12] J. E. G. J. Wijnhoven and W. L. Vos, Science **281**, 802 (1998).
[13] A. Blanco *et al.*, Nature (London) **405**, 437 (2000).
[14] Y. A. Vlasov *et al.*, Nature (London) **414**, 289 (2001).
[15] G. von Freymann *et al.*, Appl. Phys. Lett. **84**, 224 (2004).
[16] N. R. Denny *et al.*, Proc. SPIE Int. Soc. Opt. Eng. **6005**, 600505 (2005).
[17] M. Florescu *et al.*, Phys. Rev. A **72**, 033821 (2005).
[18] P. M. Bell *et al.*, Comput. Phys. Commun. **85**, 306 (1995).
[19] See EPAPS Document No. E-PRLTAO-99-033733 for supplementary text and figures. For more information on EPAPS, see http://www.aip.org/pubservs/epaps.html.
[20] D. W. Lynch and W. R. Hunter, in *Handbook of Optical Constants of Solids*, edited by E. D. Palik (Academic Press, Orlando, 1985).
[21] A. A. Krokhin and P. Halevi, Phys. Rev. B **53**, 1205 (1996).
[22] A. L. Pokrovsky *et al.*, Phys. Rev. B **71**, 165114 (2005).
[23] J. S. King *et al.*, Adv. Mater. **18**, 1063 (2006).
[24] This decrease in absorption is not due simply to a lower filling fraction of the metal. Without air cylinders, the absorption increased with decreasing filling fraction.
[25] H. F. Ghaemi *et al.*, Phys. Rev. B **58**, 6779 (1998).
[26] R. Biswas *et al.*, Phys. Rev. B **74**, 045107 (2006).